Electric field control of the photoinduced resistance increase in $La_{0.7}Sr_{0.3}MnO_3/LaTiO_3/SrTiO_3$ heterostructure

Pramod Ghising and Z. Hossain*
Department of Physics, Indian Institute of Technology, Kanpur 208016, India

(Received 19 June 2019; published 10 September 2019)

In this work we study the effect of light and electric field on the electrical properties of a $La_{0.7}Sr_{0.3}MnO_3$ film at 300 K. Taking advantage of its charge, spin, orbital, and lattice degrees of freedom, we successfully show that light and electric field together can be used to tune the resistance states of the manganite system. Using applied gate voltage V_g and light, we are able to obtain a change in resistance of about $\pm 7.5\%$. Furthermore, incorporating an ultrathin interfacial $LaTiO_3$ layer provides valuable insight into the origin of the photoinduced effect. The observed photoinduced effect is attributed to photoexcited down-spin $e_{g\downarrow}$ electrons, interfacial charge injection, and manipulation of orbital occupancy depending on the gate voltage and wavelength of light.

DOI: 10.1103/PhysRevB.100.115119

I. INTRODUCTION

In the present age of ever-evolving technology, the field of spintronics grapples to adapt with the need for efficient devices. The need of the hour is materials with multifunctional properties. Complex oxides which play host to a range of exciting phenomena, viz., high-temperature superconductivity [1], ferromagnetism [2], multiferroicity [3], and ferroelectricity [4], have taken center stage as the future of devices and technology. Ever since the discovery of high-temperature superconductivity [5], the capabilities of these oxides as an alternative for present-day semiconductor-based devices have been intensely explored. Now with the inception of various thin-film deposition techniques and the ability to fabricate heterostructures with atomically sharp interfaces, the future of oxide-based electronics seems imminent.

In this context, doped manganites have attracted a lot of attention. With their exotic phenomena like colossal magnetoresistance [6,7], ferromagnetism [2], half-metallicity [8], etc., they present a wonderful opportunity for future devices and applications. In $La_{1-x}Sr_xMnO_3$ (LSMO), the amount of Sr doping leads to a rich phase diagram and can be used to tune it to various magnetic and electrical states. Crystal field and the Jahn-Teller effect split the Mn d orbital into nondegenerate e_g ($d_{x^2-y^2}$, $d_{3z^2-r^2}$) and t_{2g} (d_{xy}, d_{yz}, and d_{xz}) orbitals [9]. Strong Hund's coupling ($J = 2$ eV) between itinerant e_g and localized t_{2g} electrons lead to parallel alignment of the Mn spins [10]. Hopping of e_g electrons between parallel aligned Mn^{3+} and Mn^{4+} ions via the double-exchange (DE) mechanism gives rise to their ferromagnetic and metallic properties [11].

Strong interplay between LSMO lattice, charge, spin, and orbital degrees of freedom leads to greater control over its various physical properties. Magnetic exchange interaction is very sensitive to e_g orbital occupancy, which can be tuned between $d_{x^2-y^2}$ and $d_{3z^2-r^2}$. In thin films, this freedom can be used to great advantage. Using strain, one can manipulate the e_g orbital occupancy (between $d_{x^2-y^2}$ and $d_{3z^2-r^2}$) to control the magnetic exchange interaction [12,13]. Electric field can also be used to tune the magnetic and electrical properties of manganites [14–16]. The sensitivity of magnetic exchange to orbital occupancy also makes light another important tuning parameter. Various photoinduced studies in manganites have shown fascinating physics spanning from persistent photoconductivity [17,18], modulation of the metal-insulator transition [19], and control of exchange bias [20] to the formation of charge-ordered clusters [21]. Due to the strong exchange interaction, photoexcited electrons have been known to alter the spin alignments in manganites, causing spin disorder in the system, widely known as the photoinduced demagnetization effect [22,23]. Thus, the use of light and electric field can be used to tune both spin and charge degrees of freedom. Here we study the effect of light and gate voltage on the electrical properties of a $La_{0.7}Sr_{0.3}MnO_3$ thin film. Introducing an ultrathin interfacial layer of $LaTiO_3$ helps to identify the mechanism behind the observed photoinduced effect. We have observed a photoinduced increase in resistance, which can be tuned with the help of gate voltage. Our observations reveal a complex interplay between optical transitions, carrier injection, and orbital occupancy.

II. EXPERIMENT

Pulsed laser ablation was used to deposit single and bilayer films of LSMO and LSMO/$LaTiO_3$ (LTO) on (001)-oriented $SrTiO_3$ (STO) substrates. Prior to film deposition, STO was etched with a NH_4HF solution to obtain a TiO_2-terminated surface. For film deposition, nanosecond pulses from an excimer laser (KrF, $\lambda = 248$ nm) were fired at the target material with a repetition rate of 2 Hz. Oxygen pressure during film deposition was maintained at 0.2 and 1×10^{-4} mbar for LSMO and LTO, respectively. X-ray diffraction with Cu $K\alpha_1$ radiation was used to confirm epitaxial growth of the films. Electrical transport measurement was done in a Quantum Design physical properties measurement system.

*zakir@iitk.ac.in

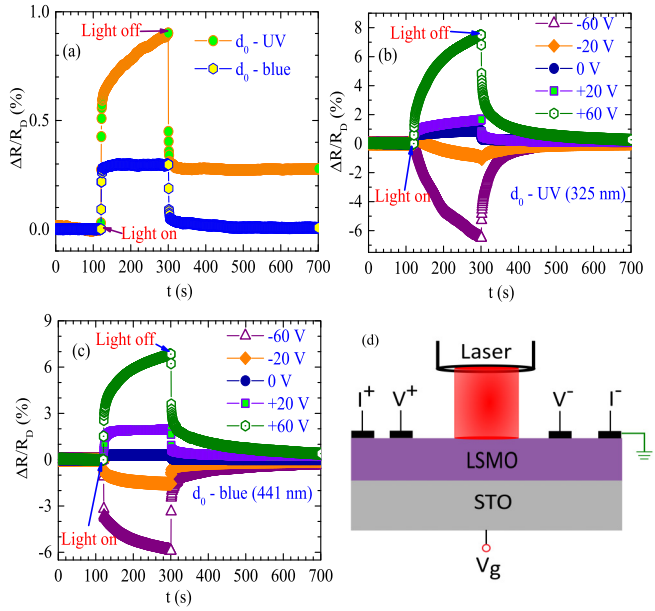

FIG. 1. Plot of percentage resistance change of sample d_0 at 300 K. (a) For UV and blue illumination at $V_g = 0$, (b) UV illumination at $V_g \neq 0$, and (c) blue illumination at $V_g \neq 0$. (d) Circuit configuration for measurement of the photoinduced effect.

Transient current measurements were done using a Keithly 237 sourcemeter. Photoresistivity measurements were carried out in a four-probe geometry with gate voltage V_g applied at the back of the STO substrate [Fig. 1(d)]. V_g was applied throughout the entire measurement, starting from $t = 0$ s for all samples. Blue (441 nm) and UV (325 nm) lines of a He-Cd continuous-wave laser with power densities of 680 and 690 mW cm^{-2}, respectively, were used for photoillumination. All the photoinduced experiments were carried out at 300 K.

III. RESULTS AND DISCUSSION

X-ray diffraction (XRD) measurements performed on the films show epitaxial growth, with only (00l)-oriented film peaks. Figure 2(a) shows the XRD plot around the (002) reflection for LSMO(15 nm)/STO and LSMO(15 nm)/LTO[10 unit cells (u.c.)]/STO (which henceforth will be called samples d_0 and d_{10}, respectively, unless otherwise stated). Both the samples exhibit metallic behavior down to 3 K, as shown in Fig. 2(b). The inset in Fig. 2(b) shows the metal-insulator transition (MIT) in the resistivity curves for samples d_0 and d_{10}. From the MIT values, the Curie temperature T_C of the LSMO films are estimated to be greater than 330 K.

The effect of photoexposure on resistivity of LSMO was studied at two wavelengths: UV ($\lambda = 325$ nm, $E_{uv} = 3.8$ eV) and blue ($\lambda = 441$ nm, $E_{\text{blue}} = 2.8$ eV) at 300 K. In manganites, due to strong spin correlation between the Mn ions, spin of the photoexcited electrons has a strong influence on its magnetic and electrical properties. For LSMO, E_{uv} and E_{blue} correspond to photoinduced down-spin (electron) transitions from O $2p$ to Mn $e_{g\downarrow}$ and between e_g orbitals on different Mn sites, respectively [23,24].

In Fig. 1 we show the percentage resistance change on exposure to UV and blue laser for sample d_0 at 300 K. An

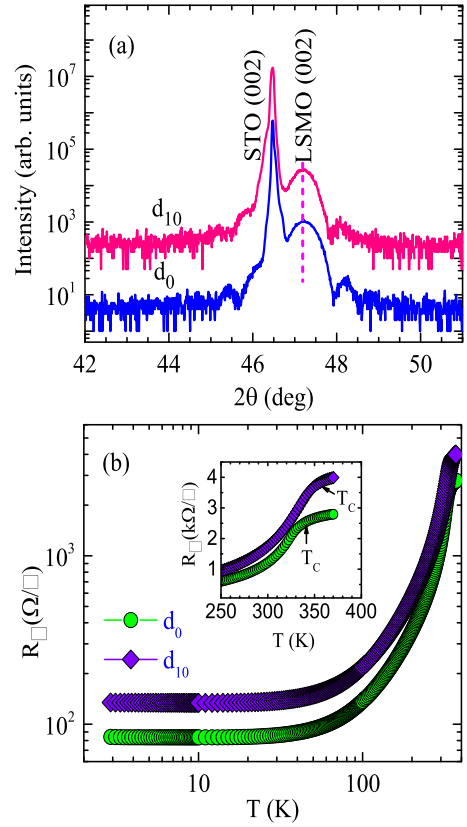

FIG. 2. Structural and electrical characterization of samples d_0 and d_{10}. (a) XRD plot showing (002) reflection of the film and the substrate. (b) Plot of sheet resistivity for samples d_0 and d_{10}. Both samples are metallic down to 3 K. The inset in (b) shows the metal-insulator transition (MIT) in the two samples. From the MIT the estimated T_C for both samples are greater than 330 K.

increase in resistance [or photoresistivity (PR)] on exposure to UV and blue light is observed at $V_g = 0$ V [see Fig. 1(a)]. Resistance change is defined as $\Delta R = R(L) - R(D)$, where $R(D)$ and $R(L)$ are resistances of the sample before and after illumination, respectively. At $T < T_C$, strong Hund's coupling ensures parallel spin alignment between itinerant e_g and localized t_{2g} electrons. Due to the strong Hund's coupling, photoexcited down-spin $e_{g\downarrow}$ electrons reverse the direction of t_{2g} spins [22], which leads to antiferromagnetic coupling between neighboring Mn ions. This spin disorder suppresses the DE-mediated electron hopping, which relies on hopping between different Mn sites with parallel t_{2g} spin alignment. Thus, photoinduced down-spin optical transitions lead to suppression of ferromagnetic correlation between the spins and, consequently, deteriorate the metallic behavior. Hence, an increase in resistance is observed on UV and blue illumination, as shown in Fig. 1(a). Another important feature of the observed photoinduced effect is the persistent behavior of PR (PPR) after photoillumination. PPR is more prominent after UV than blue illumination. In a previous report, Matsuda *et al.* [22] studied the spin dynamics in $(Nd_{0.5}Sm_{0.5})_{0.6}Sr_{0.4}MnO_3$ after $e_{g\downarrow}$ photoexcitation. They found that $e_{g\downarrow}$ excitation generates high-frequency spin waves that destroy spin correlation in the sample, which leads to spin disorder. Their pump-probe experiments revealed that even after the relaxation of $e_{g\downarrow}$

spins ($\leqslant 1$ ps), spin-wave-induced spin disorder persisted for a relatively long time ($\sim$300 ns) before the ferromagnetic ground state was recovered [22]. In the present case, as the resistivity measurement probe changes over a larger length scale (e.g., magnetic domains) [25], the observed PPR may be a result of a permanent change in the magnetic domains due to spin disorder. Also, the PPR effect shows that the observed PR is not due to thermal effects.

A much more interesting physics is observed on applying a back gate voltage V_g to the samples in concurrence with photoexposure. For a negative gate voltage electrons are pushed into the bulk of the film, away from the interface due to screening effects, whereas electrons accumulate at the film-substrate interface for a positive gate voltage [15,26]. The effect of light and gate voltage is summarized in Figs. 1(b) and 1(c) for sample d_0. In comparison to $V_g = 0$, the percentage resistivity change increases with $V_g \neq 0$ (-6.4% for $V_g = -60$ V and $+7.5\%$ for $V_g = +60$ V). Most importantly, we observe an inversion of photoresistivity for negative V_g. We believe that the inverse photoresistivity [or photoconductivity (PC)] is a result of electron injection into the LSMO film as a result of gate voltage and photoexcited electron generation in the STO substrate. We rationalize our interpretation as follows. First, the penetration depth (1/absorption coefficient) in LSMO (estimated from the absorption coefficient obtained from Fig. 2(a) of Ref. [27]) is $\sim$645 and 1818 Å for UV and blue light, respectively. As the penetration depth exceeds the film thickness (150 Å), the substrate (STO) states are also accessible for excitation to both UV and blue light. Second, STO has a band gap E_{gap} of 3.2 eV ($< E_{uv} = 3.8$ eV) [28]; hence, on exposure to UV, free electron-hole pairs are generated in STO. The negative gate voltage then serves to inject UV-generated electrons from the STO into the film. Since LSMO is half-metallic with a spin polarization of 95% [29], the injected electrons are spin polarized, which leads to the observed drop in resistivity. On the other hand, for positive V_g, the negative screening charges block the injection of UV-generated electrons into the film. However, holes generated act as traps for interfacial electrons on the LSMO side. As a result, the number of electrons available for hopping in LSMO decreases, and an increase in resistance is observed. Katsu *et al.* reported a similar electron injection at the $La_{0.8}Sr_{0.2}MnO_3$/STO interface on white-light irradiation [28]. For blue-light illumination, V_g-induced changes in resistivity of sample d_0 exhibit behavior similar to that of UV irradiation and can be seen in Fig. 1(c). We therefore envisage a similar mechanism at work here, i.e., injection of photogenerated electrons for negative V_g and trapping of conduction electrons at the interface for positive V_g. Since $E_{\text{blue}} < E_{\text{gap}}$, photogenerated electrons result from the excitation of in-gap states in STO. Photoexcitation of in-gap states (due to oxygen vacancy) in STO has been known to result in enhanced photoconductivity in oxide films [30].

To further verify the interfacial origin of the gating effect, we carry out photoinduced studies on sample d_{10}, which incorporates an insulating LTO layer at the interface. The results for UV and blue light are shown in Fig. 3. On UV irradiation, sample d_{10} exhibits photoresistivity for $V_g = 0$ as well as $V_g \neq 0$ [shown in Figs. 3(a) and 3(b)]. Another important point to take note of is the PR percentage (PR%), which is almost the same magnitude irrespective of the applied V_g (PR% $\approx +0.75\%$), as shown in Fig. 3(b). Assuming carrier injection is responsible for the observed photoinduced behavior in sample d_0, the presence of the insulating LTO layer at the interface should impede the carrier injection to some extent. For experiments carried out on sample d_{10} under UV illumination [Fig. 3(b)], PR% is independent of the applied V_g, which in turn implies V_g-aided interfacial carrier injection is indeed blocked by the LTO layer. In the absence of gate voltage sample d_0 [without the interfacial LTO layer; see Fig. 1(a)] and sample d_{10} exhibit comparable values of PR% ($\sim +0.75\%$) under UV illumination. This shows that the observed photoinduced effect in sample d_{10} is entirely due to photoexcited $e_{g\downarrow}$ transitions due to UV illumination (even under applied V_g). This observation largely supports our conjecture of interfacial charge injection under applied V_g. And when the carrier injection is blocked in sample d_{10}, only PR from the $e_{g\downarrow}$ transition is observed.

For blue light, sample d_{10} [in Fig. 3(a)] shows photoresistivity with a magnitude of PR% comparable to that of sample d_0 [in Fig. 1(a)] at $V_g = 0$. This implies blue-light-induced intersite Mn $e_{g\downarrow}$ transition is responsible for photoresistivity in sample d_{10} at $V_g = 0$. However, at $V_g \neq 0$, a peculiar behavior is observed [shown in Fig. 3(c)] which signals a different mechanism for the photoinduced effect during blue and UV illumination. At higher values of negative V_g (-60 V), photoconductivity persists. This observation indicates a different origin for the photoinduced behavior other than charge injection for blue illumination. Figure 3(d) shows the modulation of resistance on application of $V_g = -60$ V and blue illumination for sample d_{10}. V_g alone has a negligible effect on the resistance. However, light exposure in the presence of V_g shows a substantial decrease in resistance. Furthermore, only light exposure (V_g switched off) takes the sample to a resistive state. This clearly shows that photoconductivity is due to the cooperative effect of light and V_g.

Next, we study the effect of gate voltage on the photoinduced behavior in the LTO (10 u.c.)/STO film; in order to discern the contribution of the interfacial LTO layer in sample d_{10}, the results are shown in Fig. 4. The LTO/STO interface is metallic owing to the presence of a highly mobile interfacial 2D electron gas (2DEG) resulting from polar reconstruction at the interface [31,32]. The 2DEG resides in a narrow potential well formed at the interface due to bending of the STO conduction band. As shown in Fig. 4, the difference in photoinduced behavior under applied V_g for UV and blue illumination indicates two separate mechanisms for the two wavelengths. For UV illumination, photoconductivity is a direct result of generation and promotion of photoexcited electrons from the valance to conduction band in STO, which contribute electrons to the 2DEG. For blue illumination, the appearance of PC at $V_g = 0$ suggests the presence of in-gap states in STO (since $E_{\text{blue}} < E_{\text{gap}}$), which are excited by blue light. In LTO/STO the presence of oxygen vacancies V_O is responsible for the in-gap states. V_O in STO are generated due to the high gate voltages and during the film deposition process itself [33,34]. Moreover, LTO/STO films fabricated at high temperatures reportedly lead to V_O formation due to the high oxidation tendency of LTO [30,31]. V_O have been known to donate electrons to the 2DEG at the interface [35]. It

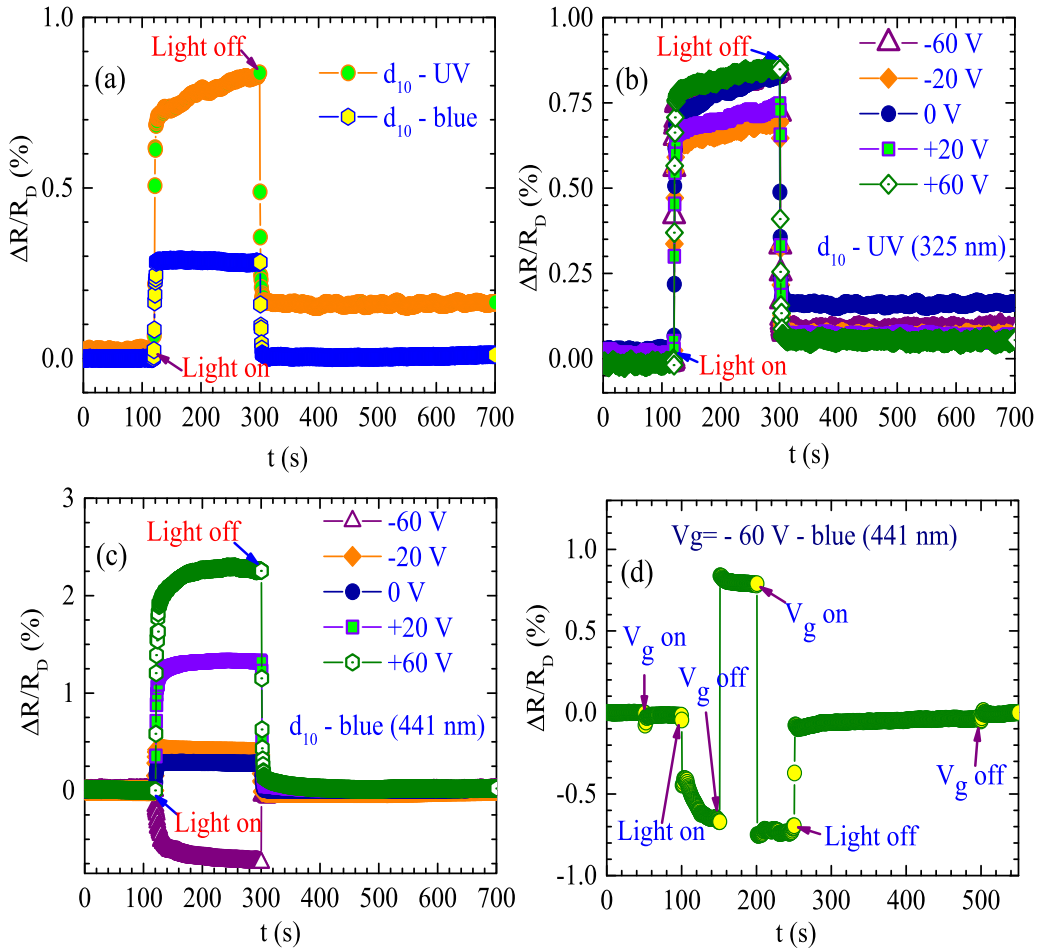

FIG. 3. Plot of percentage resistance change of sample d_{10} at 300 K. (a) For UV and blue illumination while $V_g = 0$, (b) UV illumination while $V_g \neq 0$, and (c) blue illumination while $V_g \neq 0$ and (d) resistance modulation of sample d_{10} at $V_g = -60$ V and blue illumination.

has been reported that these V_O become highly mobile under the action of light and gate voltages when trapped electrons in the V_O are photoexcited [35,36]. Thus, for negative V_g, the positively charged V_O migrate away from the interface towards the cathode (bottom of STO). Therefore, the electron contribution to 2DEG from V_O diminishes [35], leading to an increase in resistance for blue illumination. However, for positive V_g, V_O migrate towards the interface, where they donates electrons to the 2DEG, which leads to a decrease in resistance. Thus, in the presence of V_g photoinduced behavior originates

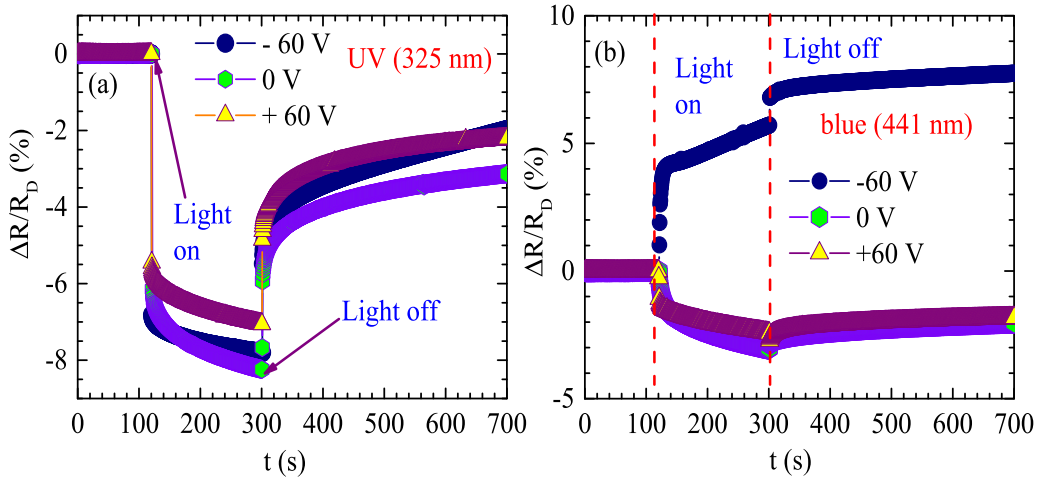

FIG. 4. Plot of percentage resistance change of the LTO (10 u.c.)/STO sample at different V_g under (a) UV illumination and (b) blue illumination.

from different mechanisms for the two wavelengths. In the following paragraphs we will discuss the role of V_O in the photoinduced behavior of LSMO.

Since e_g orbital occupancy in LSMO has tremendous influence on its magnetic and electrical properties, we need to look at the effect of V_g and photoillumination on the e_g orbital occupancy. In manganites tensile strain lowers the energy of the $d_{x^2-y^2}$ orbital with respect to the $d_{3z^2-r^2}$ orbital [37,38], which enhances its occupancy. Another factor which may also influence the orbital occupancy is V_O in STO. At room temperature, V_O in STO has been reported to be in the singly ionized state $V_O^{\bullet}$ (i.e., V_O donates one electron to the conduction band and retains the other electron) [39,40]. Photoexcitation of the in-gap states leaves V_O in a doubly ionized $V_O^{\bullet\bullet}$ state [36]. $V_O^{\bullet\bullet}$ has a lower activation energy for diffusion ($E_A = 0.6$ eV) than $V_O^{\bullet}$ ($E_A = 1$ eV) [36]; as a result the V_O diffusion process accelerates when photoexposure converts $V_O^{\bullet}$ to $V_O^{\bullet\bullet}$ [36]. In gated STO, V_O diffusion leads to accumulation of oxygen ions in the anode region and, consequently, to a polar phase with elongated TiO_6 octahedra [41]. XRD measurements have confirmed an increase in the out-of-plane lattice parameter (c) in the anode region, whereas it remains unchanged in the cathode region [41]. This result has important implications in our case; due to the outward expansion of c (along the z direction) at the STO interface resulting from V_O diffusion, MnO_6 octahedra in the LSMO overlayers will be compressed along the z direction [42]. This is akin to a tensile strain in LSMO, which lowers the $d_{x^2-y^2}$ orbital relative to $d_{3z^2-r^2}$. Thus, photoexposure and negative V_g stabilize $d_{x^2-y^2}$ orbitals. In films, in-plane correlations are much more important. Enhanced $d_{x^2-y^2}$ occupancy would boost planar exchange interaction, and so improvement in the ferromagnetic and metallic behavior is to be expected [13].

We would like to point out that the observed photoinduced effect in sample d_{10} emanates from the LSMO film and not the LTO/STO or LSMO/LTO interface. As can be seen from Figs. 3(b), 3(c), 4(a), and 4(b) the photoinduced behavior in the LTO/STO sample is in contrast to that observed in sample d_{10}, so we can rule out the contribution of the LTO/STO interface. Next, we look at the LSMO/LTO interface. This interface also presents the possibility of polar discontinuity and charge transfer, which could result in a photoinduced behavior similar to that of LTO/STO sample. In the absence of V_O in LTO, the photoinduced behavior of the LSMO/LTO should be wavelength independent. This is because the band gap of LTO ($E_{\mathrm{LTO}} = 0.2$ eV) is less than E_{uv} (3.8 eV) and E_{blue} (2.8 eV), so both UV and blue light can excite electrons from the LTO valence band to the conduction band; hence, a similar trend in photoinduced behavior would be seen for both wavelengths. However, in the case of STO, $E_{\mathrm{blue}} < E_{\mathrm{STO}} < E_{uv}$, and consequently, photoinduced behavior is different for the two wavelengths, as explained earlier. As the photoinduced behaviors for blue and UV illumination are different [see Figs. 3(b) and 3(c)] in sample d_{10}, we can exclude any contribution from the LSMO/LTO interface to the observed photoinduced effect. Furthermore, if one considers the possibility of polar discontinuity and charge transfer, the LSMO layers have a charge of $\pm 0.7e$, while the LTO layers have a charge of $\pm 1e$. Therefore, polar discontinuity dictates electron transfer at the LSMO/LTO interface. However, studies on a similar heterostructure ($LaAlO_3/La_{0.67}Sr_{0.33}MnO_3$) showed that no charge transfer occurs at such an interface [43]. This result indicates that the polar discontinuity is not strong enough to induce a charge transfer and the lattice compensates for the polar discontinuity at such an interface by some other means, i.e., structural distortions, screening of polar field by the mobile electrons in metallic LSMO, etc. A recent work by Saghayezhian *et al.* [44] also showed that the charge transfer due to polar discontinuity at the metal (LSMO)-insulator (STO) interface does not take place.

As we have already established the role of V_O diffusion in Fig. 4(b), it plays a dominant role in the observed light-induced resistivity change in sample d_{10}. When illuminated with UV ($E_{uv} > E_{\mathrm{gap}}$), carrier generation in STO involves excitation of electrons from the valence band to the conduction band, while very few or no in-gap states are excited. However, in the case of blue light ($E_{\mathrm{blue}} < E_{\mathrm{gap}}$), only in-gap states in STO are excited, which converts $V_O^{\bullet}$ to highly mobile $V_O^{\bullet\bullet}$, as explained in Ref. [36]. Thus, during blue illumination a large number of highly mobile $V_O^{\bullet\bullet}$ are generated in the STO substrate compared to UV illumination. Since V_O move due to the motion of oxygen ions in the opposite direction, they have the same mobility. During blue illumination, the large number of $V_O^{\bullet\bullet}$ easily move towards the negative V_g electrode. In response to this, oxygen ions in STO move in the opposite direction and reach the LSMO/LTO interface, diffusing through the LTO layer. The diffusion of oxygen ions through the insulating LTO layer may be facilitated by the similar structures of TiO_6 octahedra in LTO and STO. Following inspiration from the results of Hanzig *et al.* [41], accumulation of oxygen ions at the LSMO/LTO interface would polarize the LTO layer, resulting in elongated TiO_6 octahedra perpendicular to the interface (towards the LSMO overlayer). This, in turn, would increase c of the LTO layer. Consequently, MnO_6 octahedra in the LSMO overlayers will be compressed along the z direction (as the in-plane lattice parameters of the LSMO overlayer are constrained by the STO substrate) [42]. This stabilizes $d_{x^2-y^2}$ in LSMO, which leads to an increase in in-plane hopping and, consequently, to a decrease in resistance [42,45]. The observed photoconductivity at $V_g = -60$ V is due to stabilization of $d_{x^2-y^2}$, which increases electron hopping along the in-plane direction and increases the conductivity. At a lower V_g (-20 V), V_O diffusion is subdued, and the strain effect on MnO_6 octahedra vanishes. As a result, photoresistivity is dominated by intersite $e_{g\downarrow}$ transition [since PR% is comparable to that in Fig. 3(a)]. For positive V_g, $V_O^{\bullet\bullet}$ travel to the LSMO/LTO interface, which acts as traps for electrons hopping into $V_O^{\bullet\bullet}$ sites from the LSMO side. Similar studies of electron hopping across the interface and into the V_O sites were reported in oxide films [46]. This leads to a decrease in conduction electrons in the LSMO overlayers, and PR% increases with positive V_g.

In order to study the dynamics of V_O in our system, we have measured transient current in the presence of light and gate voltage. The circuit configuration for current measurement is shown in the inset of Fig. 5. A single step voltage is applied, and temporal evolution of the current is studied. In insulating titanates, oxygen vacancies are highly mobile [47]. Thus, the observed current is attributed to the diffusion of V_O in the presence of applied voltage. According to

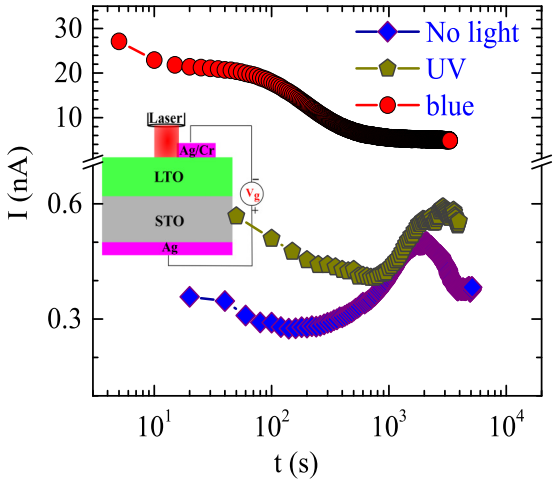

FIG. 5. Transient current measurement of the LTO(10 u.c.)/STO sample at $V_g = -60$ V. The measurements were performed under dark conditions (no illumination) and UV and blue illumination. The inset shows the measurement configuration for transient current.

space-charge-limited (SCL) theory, the transient current exhibits a peak which is directly related to the mobility of the injected charge species [47]. Figure 5 shows current as a function of time after a single step voltage ($V_g = -60$ V) is applied to the bottom electrode. The peak in the $I(t)$ curve determines the mobility of V_O during and in the absence of illumination. According to SCL theory, the peak position τ_p is related to the mobility μ as follows [47]:

$$\tau_p = \frac{0.78d^2}{\mu V_g}, \tag{1}$$

where d is the sample thickness. The value of μ can be estimated from Eq. (1); the calculated values of μ are 5.0×10^{-7} cm^2 V^{-1} s^{-1} for blue illumination, 1.5×10^{-8} cm^2 V^{-1} s^{-1} for UV illumination, and 1.7×10^{-8} cm^2 V^{-1} s^{-1} for no light. As can be seen, while μ is of the same order for UV and no light, it increases by an order of magnitude for blue light. Thus, for blue light, generation of highly mobile $V_O^{\bullet\bullet}$ due to photoexcitation of in-gap states leads to the observed photoconductivity in sample d_{10}. On the other hand, UV illumination generates a large number of mobile electrons in STO rather than $V_O^{\bullet\bullet}$, whose injection into the LSMO layer is blocked by the insulating LTO layer. As a result, UV illumination produces no changes in photoinduced behavior with applied V_g in sample d_{10}. Finally, now that we have established the role of $V_O^{\bullet\bullet}$ in the photoinduced effect, it is reasonable to suggest that the photoinduced effect of sample d_0 (under blue illumination) originates from $V_O^{\bullet\bullet}$ diffusion and electron injection.

IV. CONCLUSIONS

In summary, we have studied the photoinduced effect on LSMO films at 300 K. Under UV and blue-light exposure, depending on the sign of the applied gate voltage, both photoresistivity and photoconductivity are observed. While, at $V_g = 0$, spin disorder in LSMO induced by the $e_{g\downarrow}$ photoexcited transition is the dominant mechanism for photoresistivity, for $V_g \neq 0$ interfacial charge injection and oxygen vacancy diffusion play a pivotal role in the photoinduced behavior. Under UV illumination, photoinduced behavior at $V_g \neq 0$ stems from the injection of photoexcited electrons generated in the STO substrate. As a result, introducing an ultrathin layer of LTO at the LSMO/STO interface inhibits this carrier injection process, and only photoresistivity from the photoexcited $e_{g\downarrow}$ transition is observed (even for $V_g \neq 0$). However, for blue illumination, the observation of photoconductivity (at high $-V_g$) even in the presence of the interfacial LTO layer suggests the role of oxygen vacancy diffusion in the observed photoinduced effect at $V_g \neq 0$. Light- and gate-voltage-driven diffusion of oxygen vacancy in these heterostructure alters the orbital occupancy of e_g electrons in the LSMO overlayer. In this work we have shown that using light and electric field, one can simultaneously control the orbital and charge degrees of freedom in the LSMO/LTO/STO heterostructure.

ACKNOWLEDGMENTS

The authors would like to thank R. C. Budhani and S. Middey for the valuable discussions. Financial support from IIT Kanpur is gratefully acknowledged.

[1] A. Schilling, M. Cantoni, J. D. Guo, and H. R. Ott, Nature (London) **363**, 56 (1993).
[2] G. Jonker and J. V. Santen, Physica **16**, 337 (1950).
[3] R. Ramesh and N. A. Spaldin, Nat. Mater. **6**, 21 (2007).
[4] M. Acosta, N. Novak, V. Rojas, S. Patel, R. Vaish, J. Koruza, G. A. Rossetti, and J. Rödel, Appl. Phys. Rev. **4**, 041305 (2017).
[5] J. G. Bednorz and K. A. Müller, Z. Phys. B **64**, 189 (1986).
[6] R. von Helmolt, J. Wecker, B. Holzapfel, L. Schultz, and K. Samwer, Phys. Rev. Lett. **71**, 2331 (1993).
[7] S. Jin, T. H. Tiefel, M. McCormack, R. A. Fastnacht, R. Ramesh, and L. H. Chen, Science **264**, 413 (1994).
[8] J.-H. Park, E. Vescovo, H.-J. Kim, C. Kwon, R. Ramesh, and T. Venkatesan, Nature (London) **392**, 794 (1998).
[9] A.-M. Haghiri-Gosnet and J.-P. Renard, J. Phys. D. **36**, R127 (2003).
[10] Y. Moritomo, A. Machida, K. Matsuda, M. Ichida, and A. Nakamura, Phys. Rev. B **56**, 5088 (1997).
[11] C. Zener, Phys. Rev. **82**, 403 (1951).
[12] Y. Konishi, Z. Fang, M. Izumi, T. Manako, M. Kasai, H. Kuwahara, M. Kawasaki, K. Terakura, and Y. Tokura, J. Phys. Soc. Jpn. **68**, 3790 (1999).
[13] A. Sadoc, B. Mercey, C. Simon, D. Grebille, W. Prellier, and M.-B. Lepetit, Phys. Rev. Lett. **104**, 046804 (2010).
[14] B. Cui, C. Song, G. A. Gehring, F. Li, G. Wang, C. Chen, J. Peng, H. Mao, F. Zeng, and F. Pan, Adv. Funct. Mater. **25**, 864 (2015).
[15] A. S. Dhoot, C. Israel, X. Moya, N. D. Mathur, and R. H. Friend, Phys. Rev. Lett. **102**, 136402 (2009).
[16] F. A. Cuellar, Y. H. Liu, J. Salafranca, N. Nemes, E. Iborra, G. Sanchez-Santolino, M. Varela, M. G. Hernandez, J. W.

Freeland, M. Zhernenkov, M. R. Fitzsimmons, S. Okamoto, S. J. Pennycook, M. Bibes, A. Barthélémy, S. G. E. te Velthuis, Z. Sefrioui, C. Leon, and J. Santamaria, Nat. Commun. **5**, 4215 (2014).

[17] R. Cauro, A. Gilabert, J. P. Contour, R. Lyonnet, M.-G. Medici, J.-C. Grenet, C. Leighton, and I. K. Schuller, Phys. Rev. B **63**, 174423 (2001).

[18] J. M. Dai, W. H. Song, S. G. Wang, K. Y. Wang, S. L. Ye, J. J. Du, and Y. P. Sun, J. Appl. Phys. **89**, 6967 (2001).

[19] N. Takubo, I. Onishi, K. Takubo, T. Mizokawa, and K. Miyano, Phys. Rev. Lett. **101**, 177403 (2008).

[20] K. D. Sung, T. K. Lee, and J. H. Jung, Nanoscale Res. Lett. **10**, 125 (2015).

[21] X. J. Liu, Y. Moritomo, A. Machida, A. Nakamura, H. Tanaka, and T. Kawai, Phys. Rev. B **63**, 115105 (2001).

[22] K. Matsuda, A. Machida, Y. Moritomo, and A. Nakamura, Phys. Rev. B **58**, R4203 (1998).

[23] X. Liu, A. Machida, Y. Moritomo, M. Ichida, and A. Nakamura, Jpn. J. Appl. Phys. **39**, L670 (2000).

[24] M. Quijada, J. Černe, J. R. Simpson, H. D. Drew, K. H. Ahn, A. J. Millis, R. Shreekala, R. Ramesh, M. Rajeswari, and T. Venkatesan, Phys. Rev. B **58**, 16093 (1998).

[25] X. J. Liu, Y. Moritomo, A. Nakamura, and H. Asano, Jpn. J. Appl. Phys. **39**, L1233 (2000).

[26] A. Rastogi, J. J. Pulikkotil, and R. C. Budhani, Phys. Rev. B **89**, 125127 (2014).

[27] M. Cesaria, A. Caricato, G. Leggieri, M. Martino, and G. Maruccio, Thin Solid Films **545**, 592 (2013).

[28] H. Katsu, H. Tanaka, and T. Kawai, Appl. Phys. Lett. **76**, 3245 (2000).

[29] M. Bowen, M. Bibes, A. Barthelemy, J.-P. Contour, A. Anane, Y. Lemaître, and A. Fert, Appl. Phys. Lett. **82**, 233 (2003).

[30] A. Rastogi and R. C. Budhani, Opt. Lett. **37**, 317 (2012).

[31] A. Rastogi, J. J. Pulikkotil, S. Auluck, Z. Hossain, and R. C. Budhani, Phys. Rev. B **86**, 075127 (2012).

[32] P. Ghising, D. Das, S. Das, and Z. Hossain, J. Phys.: Condens. Matter **30**, 285002 (2018).

[33] A. Kalabukhov, R. Gunnarsson, J. Börjesson, E. Olsson, T. Claeson, and D. Winkler, Phys. Rev. B **75**, 121404(R) (2007).

[34] K. T. Kang, H. Kang, J. Park, D. Suh, and W. S. Choi, Adv. Mater. **29**, 1700071 (2017).

[35] Y. Lei, Y. Li, Y. Z. Chen, Y. W. Xie, Y. S. Chen, S. H. Wang, J. Wang, B. G. Shen, N. Pryds, H. Y. Hwang, and J. R. Sun, Nat. Commun. **5**, 5554 (2014).

[36] Y. Li, Y. Lei, B. G. Shen, and J. R. Sun, Sci. Rep. **5**, 14576 (2015).

[37] M. Huijben, L. W. Martin, Y.-H. Chu, M. B. Holcomb, P. Yu, G. Rijnders, D. H. A. Blank, and R. Ramesh, Phys. Rev. B **78**, 094413 (2008).

[38] C. Aruta, G. Ghiringhelli, A. Tebano, N. G. Boggio, N. B. Brookes, P. G. Medaglia, and G. Balestrino, Phys. Rev. B **73**, 235121 (2006).

[39] D. D. Cuong, B. Lee, K. M. Choi, H.-S. Ahn, S. Han, and J. Lee, Phys. Rev. Lett. **98**, 115503 (2007).

[40] C. Lin and A. A. Demkov, Phys. Rev. Lett. **111**, 217601 (2013).

[41] J. Hanzig, M. Zschornak, F. Hanzig, E. Mehner, H. Stöcker, B. Abendroth, C. Röder, A. Talkenberger, G. Schreiber, D. Rafaja, S. Gemming, and D. C. Meyer, Phys. Rev. B **88**, 024104 (2013).

[42] H. Chen, Q. Qiao, M. S. J. Marshall, A. B. Georgescu, A. Gulec, P. J. Phillips, R. F. Klie, F. J. Walker, C. H. Ahn, and S. Ismail-Beigi, Nano Lett. **14**, 4965 (2014).

[43] Y. Z. Chen, F. Trier, T. Wijnands, R. J. Green, N. Gauquelin, R. Egoavil, D. V. Christensen, G. Koster, M. Huijben, N. Bovet, S. Macke, F. He, R. Sutarto, N. H. Andersen, J. A. Sulpizio, M. Honig, G. E. D. K. Prawiroatmodjo, T. S. Jespersen, S. Linderoth, S. Ilani, J. Verbeeck, G. Van Tendeloo, G. Rijnders, G. A. Sawatzky, and N. Pryds, Nat. Mater. **14**, 801 (2015).

[44] M. Saghayezhian, S. Kouser, Z. Wang, H. Guo, R. Jin, J. Zhang, Y. Zhu, S. T. Pantelides, and E. W. Plummer, Proc. Natl. Acad. Sci. USA **116**, 10309 (2019).

[45] H.-J. Liu, T.-C. Wei, Y.-M. Zhu, R.-R. Liu, W.-Y. Tzeng, C.-Y. Tsai, Q. Zhan, C.-W. Luo, P. Yu, J.-H. He, Y.-H. Chu, and Q. He, Adv. Funct. Mater. **26**, 729 (2016).

[46] S. Wu, L. Ren, J. Qing, F. Yu, K. Yang, M. Yang, Y. Wang, M. Meng, W. Zhou, X. Zhou, and S. Li, ACS Appl. Mater. Interfaces **6**, 8575 (2014).

[47] S. Zafar, R. E. Jones, B. Jiang, B. White, P. Chu, D. Taylor, and S. Gillespie, Appl. Phys. Lett. **73**, 175 (1998).